Convolutional Neural Network-based Reconstruction for Positronium Annihilation Localization

Jin Jegal
Kyungpook National University
Dongwoo Jeong
Kyungpook National University
Eun-Suk Seo
University of Maryland, College Park
HyeoungWoo Park (hyeoung87@gmail.com)
Kyungpook National University
Hongjoo Kim
Kyungpook National University

Research Article

Keywords: hermetic novel, Bismuth germanium oxide crystal scintillators, tumor localization, CNN

Posted Date: January 7th, 2022

DOI: https://doi.org/10.21203/rs.3.rs-1216054/v1

Abstract

A hermetic novel detector composed of 200 Bismuth germanium oxide crystal scintillators and 393 channel silicon photomultipliers has been developed for positronium (Ps) annihilation study. This compact 4π detector is capable of simultaneously detecting γ-ray decay in all directions, enabling not only the study of visible and invisible exotic decay processes but also tumor localization in positron emission tomography for small animals. In this study, we investigate the use of a convolutional neural network (CNN) for the localization of the Ps annihilation synonymous with tumor localization. The 2-γ decay systems of the Ps annihilation from the ^{22}Na and ^{18}F radioactive sources are simulated using GEANT4. The simulated data sets are preprocessed by applying energy cuts. The spatial error in the XY plane from CNN is compared to that from the classical centroiding, weighted k-means algorithm. The feasibility of the CNN-based Ps an-nihilation reconstruction with tumor localization is discussed.

Introduction

Among various deep learning models, convolutional neural networks (CNNs) have been established as the most entrenched algorithm due to their successful results at the ImageNet Large Scale Visual Recognition Competition in 2012[1]. CNNs can directly learn feature vectors from the training datasets by continuously updating weight by decreasing the loss index[2]. One of the advantages of CNNs over conventional machine learning is the provision of a higher-level concept of expressing semantic insights about data domains by architectural design choices in the computational graph. However, to achieve this advantage, sufficient data and computation time are needed[3]. Fortunately, this limitation can be overcome by the application of Graphics Processor Units to an Artificial intelligence platform, which accelerates the development of deep learning models as well as CNNs[4]. Moreover, they have been developed and utilized in various fields, such as vision-based detection[5], probability inference[6,7], and medical image segmentation[8,9].

CNN-based data reconstruction has been especially successful when utilized for charged particle tracking with good precision in accelerator and calorimeter experiments[10–12]. Additionally, CNN has effectively overcome the spatial resolution limitations of positron emission tomography (PET), which was essentially limited by the size of the detector array elements, such as the crystal scintillator and readout pixels used in medical imaging[13]. These high-performance results can be obtained through Monte Carlo (MC) simulations which can generate sufficient training data and represents the geometry of the detector well. Consequently, CNN is expected to be suitable for analyzing large amounts of data for background noise cut-off in the Kyungpook National University Advanced Positronium Annihilation Experiment (KAPAE) detector.

KAPAE, which is a 4π detector, comprises 200 $Bi_4Ge_3O_{12}$ (BGO) crystal scintillators and 393 channels of silicon photomultipliers (SiPM). In the KAPAE detector, a ^{22}Na radioactive source is used to generate positrons from $\beta+$ decay. The instrument configuration is optimized to trigger on positrons by varying the

polyethylene naphthalate (PEN) film plastic scintillator thickness[14]. KAPAE aims to study CPT-violation in positronium (Ps) annihilation physics[14,15]. Based on the relative spin orientations, the ground state of Ps has two possible configurations: the triplet state ($^3S_1$), ortho positronium (o-Ps), and the singlet state ($^1S_0$), para positronium (p-Ps). Due to C-parity conservation, p-Ps and o-Ps decay to even and odd numbers of photons, respectively. Since these processes possess different C-parity values, the precise distinction of p-Ps and o-Ps is important to test discrete symmetries of C, CP, and CPT in the lepton sector[16].

In this study, data reconstruction based on a CNN focusing on the back-to-back 2-γ decay system is conducted. The 2-γ energies are deposited in the surrounding BGO scintillators, and this process is simulated by the GEANT4 simulation toolkit[17]. The simulation data are used to produce datasets for reconstructions based on the CNN and weighted k-means algorithm[18]. The k-means clustering algorithm is a conventional method to determine the clustering centroid for uncategorical datasets typically, and it had been utilized in the abovementioned fields of CNN applications. Through this 2-γ decay system data reconstruction, we can distinguish the p-Ps signal from the o-Ps signal for the background noise cut-off and detect o-Ps events more correctly with high efficiency. Also note that the size of the KAPAE detector is compact (150 × 150 × 150 mm^3) and it can simultaneously detect γ-ray decays in all directions. This feature makes it possible to utilize the KAPAE detector with an ^{18}F radioactive source in PET application for tumor localization of small animals[19].

Results

Energy cut-off criterion

Four sets of data corresponding to various energy cuts centered at 511 keV are used to train data. In Table 1, the “1σ” and “2σ” are the energy cut between ± 1σ and ± 2σ centered at 511 keV and “>2σ” is the energy cut ranges of more than 2σ, 0.6 MeV. The number of events varies corresponding to the energy cut ranges as shown in Fig. 1. However, as we maintain the batch size to 3% of the dataset for the same number of interactions in each case, these 4 sets can be compared to find out how different energy cut ranges affect the reconstruction.

Table 1
XY RMSE [mm] of Ps annihilation localization by CNN-based reconstruction depending on the energy cut-off criteria.

Radioactive source	1σ	2σ	>2σ	Not applied
^{22}Na	4.69	4.52	4.19	4.17
^{18}F	4.53	4.33	3.93	3.88

The root mean square error (RMSE) of Ps annihilation localization by CNN depending on energy cut criterion and radioactive sources is summarized in Table 1. The RMSE is calculated by comparing the XY coordinates of Ps in each event from the GEANT4 simulation (true) with the reconstruction position based on CNN (predicted). In the test data, 100,000 events are used for calculating the RMSE. Since the X and Y coordinate are not correlated, the RMSE is calculated all at once. As shown in Table 1, when σ is increased to include the low energy contribution from Compton scattering, the spatial error in the XY plane decreases. In addition, when 1.28 MeV γ-rays from the ^{22}Na source is included, the RMSE is further decreased. However, the reconstructed position is closer to the true value for the smaller σ cases where 1.28 MeV γ-ray events are not included as shown in Fig. 2. This means that the inclusion of the correlated information to the 2-γ decay is helpful for training the CNN model. For the 1σ and 2σ cases, there are peaks between ± 5.0 mm and ± 7.5 mm resulting in lower accuracy than other cases. Therefore, the optimized energy cut-off criterion for the back-to-back 2-γ decay system discrimination modeling is determined as "> 2σ", where the spatial error in XY is 4.19 mm for ^{22}Na and 3.93 mm for ^{18}F.

The CNN performance

The Ps annihilation localization performances of CNN is compared with the classical centroiding weighted k-means algorithm. The "> 2σ" energy cut-off is used to achieve the best accuracy in the XY plane. The RMSE between the simulated XY position of Ps annihilation and that predicted by CNN is calculated. It is compared with the RMSE for the weighted k-means clustering algorithm in Table 2. The RMSE from the CNN with our proposed architecture is 2.2 times smaller than that from the weighted k-means clustering algorithm.

Table 2
The RMSE [mm] of Ps localization based on the weighted k-means algorithm and the CNN-based reconstruction corresponding to radioactive source.

Radioactive source	The weighted k-means algorithm	The CNN
^{22}Na	9.42	4.19
^{18}F	8.49	3.93

Figure 3 shows the Ps annihilation localization from CNN and weighted k-means clustering; they are compared with the true position from the GEANT4 simulation data in the case of ^{18}F. In GEANT4 simulation data, most positrons are generated from β + decay of a radioactive source. Since the radioactive source is located at the center of the trigger system, (0,0) mm in XY plane, most of the Ps annihilates in the trigger space within ±7.5 mm (XY) (Fig. 4). In addition, an increase in the number of Ps annihilations at the edge of the trigger space near ±7.5 mm (XY) is due to the positron diffraction in the solid BGO crystal[20]. The weighted k-means algorithm is repeatedly trained to determine the clustering centroid until the distance between the centroid and its adjacent components is minimized. In contrast, the CNN is optimized to directly minimize the error by comparing the true position data until the results

converge to a minimum loss index. The CNN can adapt to various circumstances even with the irregular data set information by updating weight. Consequently, the CNN results (Fig. 3) show that the reconstructed Ps annihilation localization is more accurate than the weighted k-means clustering-based.

Discussion

This study has performed CNN-based Ps annihilation reconstruction using the KAPAE detector and compared the results with a conventional weighted k-means algorithm. The detector geometry and back-to-back 2-γ decay system produced by p-Ps annihilation is simulated by using GEANT4. ^{22}Na and ^{18}F radioactive sources are used for CPT-violation study and PET application. The energy cut-off criterion of over 2σ is determined by comparing the RMSEs. For ^{22}Na, using the weighted k-means algorithm and CNN, Ps annihilation is reconstructed with a RMSE of 9.42 mm and 4.19 mm, respectively. For ^{18}F, using the weighted k-means algorithm and CNN, Ps annihilation is reconstructed with a RMSE of 8.49 and 3.93 mm, respectively. In conclusion, the proposed CNN architecture achieved about two times better spatial resolution in the XY plane compared to the weighted k-means algorithm. Thus, this proposed CNN architecture can be applied to distinguish p-Ps from o-Ps for CPT violation study from subsequent γ energy deposited on BGO scintillators as well as to localize the tumor position in PET for small animals.

Methods

Monte Carlo simulation

Figure 4 shows the GEANT4 simulation of the radioactive decay from a ^{22}Na or ^{18}F point source in the KAPAE detector. The simulated detector comprises 192 BGO scintillators with dimensions of 7.5 × 7.5 × 150 mm^3 and 8 endcap BGO scintillators with dimensions of 7.5 × 7.5 × 50 mm^3 surrounding the trigger system. Each scintillator is covered by a VM2000 reflector of 75 μm thickness. The point source is placed at the center of the PEN film plastic scintillator. It is represented by a yellow box in the middle of Fig. 4. The KAPAE detector is filled with nitrogen gas and a silica aerogel is used for generation of o-Ps annihilation for minimization of a pick-off effect[14]. We simulate the 2-γ system of p-Ps signals only because we can discriminate o-Ps in real data by developing the p-Ps data reconstruction model. The real data for the γ energy spectrum from the BGO scintillator is taken by SiPMs attached to both ends of the KAPAE detector. Instead of replicating all SiPMs in the simulation, just the SiPM photon detection efficiency from the experiment is considered in the simulation.

One million events of the 2-γ decay system of p-Ps are initially generated for discrimination with o-Ps in real data, and only events passing through the trigger system are selected. The pseudo data are processed using the scintillation energy resolution in the BGO scintillator scintillation from a preliminary experiment by utilizing the SiPM. The total statistical noise fluctuation (σ/E) is proportional to $(1/\sqrt{n})$, given by the Poisson distribution as follows:

$$\frac{\sigma}{E} = k\frac{1}{\sqrt{n}}$$

1

where k is the proportional constant, n = L × E × PDE is the number of photons, L is the absolute light yield of the scintillator (photons/MeV), E is the energy (MeV), and PDE is the scintillation light detection efficiency of the SiPM. The pseudo data of ^{22}Na and ^{18}F are processed using Equation (1). The energy spectra of 511 keV γ-rays from both sources are shown in Fig. 5. The full width at half maximum (FWHM) is 24% for each source.

The pseudo data are written in Python for the machine learning framework and processed to a matrix of pixels corresponding to the BGO scintillator array position mapping. The data are restructured to a 14 × 14 matrix for the top view of the detector. The central 4 × 4 data are from the deposited energy of the short 8 endcap BGO scintillators. The 4 endcap scintillators above the trigger system are paired with the 4 endcap scintillators below the trigger system. The energy deposit sum of each pair forms the central 4 × 4 data. Four sets of data corresponding to various energy cuts centered at 511 keV are used to train data (Table 3).

Table 3
The number of events corresponding to the energy cut ranges.

Radioactive source	1σ	2σ	>2σ	Not applied
^{22}Na	394,839	467,378	520,228	536,256
^{18}F	427,965	506,384	549,850	550,540

Weighted K-means algorithm

To evaluate the CNN performance, the conventional weighted k-means algorithm[21] is also utilized. The k-means algorithm employs an iterative approach to group the data into k predetermined clusters by minimizing the sum of squared errors (SSE). The SSE is obtained as follows:

$$SSE = \sum_{i=1}^{n}\sum_{j=1}^{k} w^{(i,j)}\|x^{(i)} - \mu^{(j)}\|^{q}$$

2

where $\mu^{(j)}$ is the centroid of the jth cluster, $x^{(i)}$ is the data sample, k is the number of clusters, n is the number of elements on the data set, and q is an integer that defines the nature of the distance function (q is 2 for the Euclidean distance). Further, $\mu^{(j)}$ is 1 if the data sample $x^{(i)}$ belongs to the jth cluster and 0 otherwise. The weighted k-means algorithm is utilized in the scikit-learn package. Unlike CNN data, the center XY position of the BGO scintillator deposited with γ energy is used as the data. Each position has

weight corresponding to the deposited γ energy of the BGO scintillator. Since a radioactive source is centered on the detector, k is set as 1, and the Ps annihilation position will be biased by the γ energy.

CNN

- CNN architecture

The proposed CNN architecture is initialized by using Keras 2.1.6 with Tensorflow 2.4.0 as a backend in Python 3.8.5[22]. The network architecture (Fig. 6) comprises two convolutional layers as feature extraction and the output dense layer. Various architectures are set up and tested, and the number of convolutional, pooling, and fully connected layers and the number of filters in each layer are determined. Starting with the 14 × 14 input shape, Rectified Linear Unit (ReLU) activation, defined as $f(x) = \max(x, 0)$[23], is performed for each functional layer, including the dense layer. For regression, a linear activation is performed at the end of the dense layer in order to output the 2D coordinates (XY) of the Ps annihilation position as a 1 × 2 vector.

- Model training and testing

MC simulation data of the 2-γ decay of the ^{22}Na and ^{18}F radioactive sources are employed for the training. By utilizing GEANT4 and excluding the empty matrix data where all components are 0, sufficient events are generated to train the CNN. The CNN training is performed by using 70% of the dataset, and the remaining 30% of the dataset is used for training validation. As an optimizer, Nesterov-accelerated adaptive moment estimation (Nadam)[24] is used for training optimization with an initial learning rate of 0.001. Nadam is an advanced optimizer with the Nesterov accelerated gradient added to the adaptive moment estimation (Adam)[25]. Moreover, it can advantageously find the global minimum more quickly and accurately than Adam by determining the gradient after moving to the momentum value rather than determining the gradient and momentum values to move from the current position to the next position[26]. Mean squared error (MSE) is used as the loss metric. The batch size is adapted to maintain the batch size as 3% of the dataset, and the number of epochs is optimized to the epoch just before overfitting occurs. Then, the model converges in the direction of minimizing the MSE and mean absolute error as a function of epochs. These loss curves reach approximately equal minimums with asymptotic behavior. The remaining 30% of the dataset is used for testing the model.

Declarations

Acknowledgements

This research was supported by the MSIT (Ministry of Science, ICT), Korea, under the High-Potential Individuals Global Training Program (2021-0-01544) supervised by the IITP (Institute for Information & Communications Technology Planning & Evaluation) and the National Research Foundation of Korea

(NRF) funded by the Ministry of Education, Korea (no. 2020R1A6A3A01099805 and 2021R1A2B5B0300200611).

References

1. Yamashita, R., Nishio, M., Do, R. K. G. & Togashi, K. Convolutional neural networks: an overview and application in radiology. *Insights into imaging* **9**, 611-629 (2018).
2. Driss, S. B., Soua, M., Kachouri, R. & Akil, M. A comparison study between MLP and convolutional neural network models for character recognition. in *Real-Time Image and Video Processing* 2017. **1022306** (International Society for Optics and Photonics).
3. Aggarwal, C. C. Neural networks and deep learning. *Springer* **10**, 978-973 (2018).
4. Potluri, S., Fasih, A., Vutukuru, L. K., Al Machot, F. & Kyamakya, K. in Proceedings of the Joint INDS'11 & ISTET'11. 1-7 (IEEE).
5. Bappy, J. H. & Roy-Chowdhury, A. K. CNN based region proposals for efficient object detection. in 2016 *IEEE International Conference on Image Processing (ICIP)*. 3658-3662 (IEEE).
6. Raina, K. Statistical inference of the inter-sample Dice distribution for discriminative CNN brain lesion segmentation models. arXiv:2012.02755 (2020).
7. Zhou, Y. & Liang, H. Statistical inference for semiparametric varying-coefficient partially linear models with error-prone linear covariates. *The Annals of Statistics* **37**, 427-458 (2009).
8. Karimi, D. & Salcudean, S. E. Reducing the hausdorff distance in medical image segmentation with convolutional neural networks. *IEEE Transactions on medical imaging* **39**, 499-513 (2019).
9. Kayalibay, B., Jensen, G. & van der Smagt, P. CNN-based segmentation of medical imaging data. arXiv:1701.03056 (2017).
10. Sharma, R. K. & Gabrani, G. Exploring Deep Learning Methods for Particle Track Reconstruction. in 2019 *19th International Conference on Computational Science and Its Applications (ICCSA)*. 120-125 (IEEE).
11. Belayneh, D. et al. Calorimetry with deep learning: particle simulation and reconstruction for collider physics. *The European Physical Journal C* **80**, 1-31 (2020).
12. Erdmann, M., Glombitza, J. & Walz, D. A deep learning-based reconstruction of cosmic ray-induced air showers. *Astroparticle Physics* **97**, 46-53 (2018).
13. LaBella, A., Vaska, P., Zhao, W. & Goldan, A. H. Convolutional neural network for crystal identification and gamma ray localization in PET. *IEEE Transactions on Radiation and Plasma Medical Sciences* **4**, 461-469 (2020).
14. Jeong, D. W., Khan, A., Park, H. W., Lee, J. & Kim, H. Optimization and characterization of detector and trigger system for a KAPAE design. *Nuclear Instruments and Methods in Physics Research Section A: Accelerators, Spectrometers, Detectors and Associated Equipment* **989**, 164941 (2021).
15. Park, H., Jung, D., Hwang, S. & Kim, H. Design of novel compact detector based on the bismuth germanate scintillator and silicon photomultiplier for ortho-positronium physics. *Acta Physica*

Polonica B **51**, 143 (2020).

16. Bass, S. D. QED and fundamental symmetries in positronium decays. arXiv:1902.01355 (2019).
17. Agostinelli, S. et al. GEANT4—a simulation toolkit. *Nuclear Instruments and Methods in Physics Research Section A: Accelerators, Spectrometers*, *Detectors and Associated Equipment* **506**, 250–303 (2003).
18. MacQueen, J. Some methods for classification and analysis of multivariate observations. in *Proceedings of the fifth Berkeley symposium on mathematical statistics and probability*. 281-297 (Oakland, CA, USA).
19. Endo, K. et al. PET and PET/CT using 18 F-FDG in the diagnosis and management of cancer patients. *International journal of clinical oncology* **11**, 286-296 (2006).
20. Hugenschmidt, C. Positrons in surface physics. *Surface Science Reports* **71**, 547–594 (2016).
21. Ahmad, A. & Dey, L. A k-mean clustering algorithm for mixed numeric and categorical data. *Data & Knowledge Engineering* **63**, 503-527 (2007).
22. Keras-team, K. D. The python deep learning library. Available (accessed 5 May 2019): https://keras.io.
23. Hinton, G. E. Rectified linear units improve restricted boltzmann machines vinod nair. in *27th International Conference on Machine Learning (ICML).* (2010).
24. Dozat, T. Incorporating nesterov momentum into adam. in *ICLR Workshop* (2016).
25. Kingma, D. P. & Ba, J. Adam: A method for stochastic optimization. arXiv:1412.6980 (2014).
26. Ruder, S. An overview of gradient descent optimization algorithms. arXiv:1609.04747 (2016).

Figures

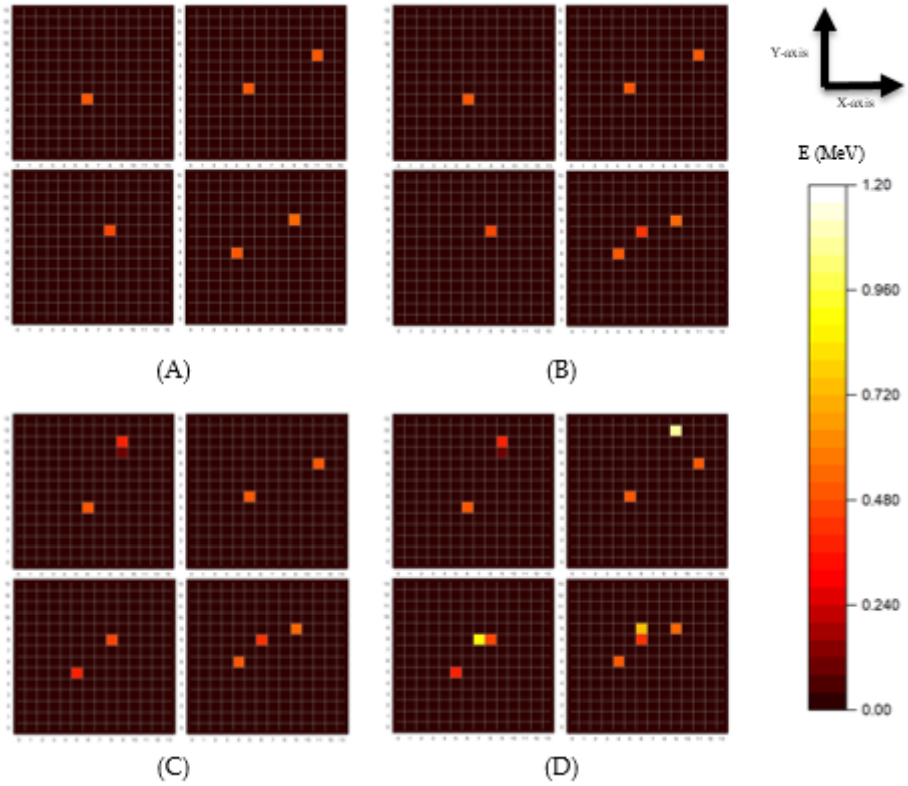

Figure 1

The γ energy distribution of a top view of the BGO scintillators. -An example of randomly selected 4 events are compared for 4 different energy cutoff ranges given in Table 1: (A) 1σ (B) 2σ (C) above 2σ, and (D) no cut-off.

Figure 2

Difference between reconstructed and true Ps annihilation position corresponding to energy cut-off range of (A) ^{22}Na and (B) ^{18}F.

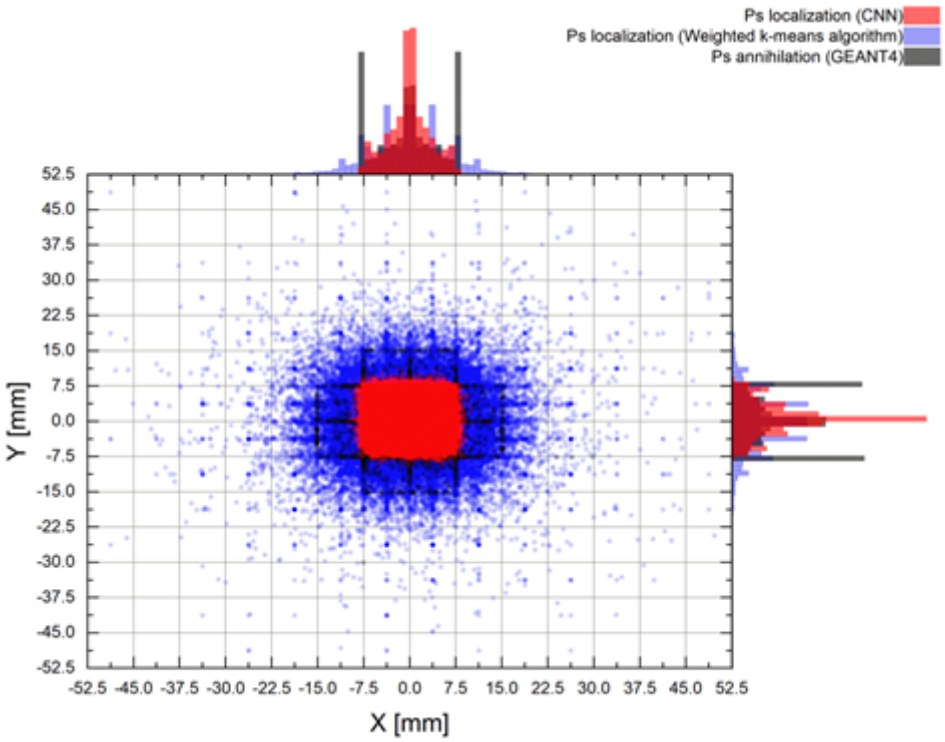

Figure 3

The obtained Ps annihilation localizations for the case of ^{18}F using the CNN and the weighted k-means algorithm; the XY coordinates are for the top view of the KAPAE detector.

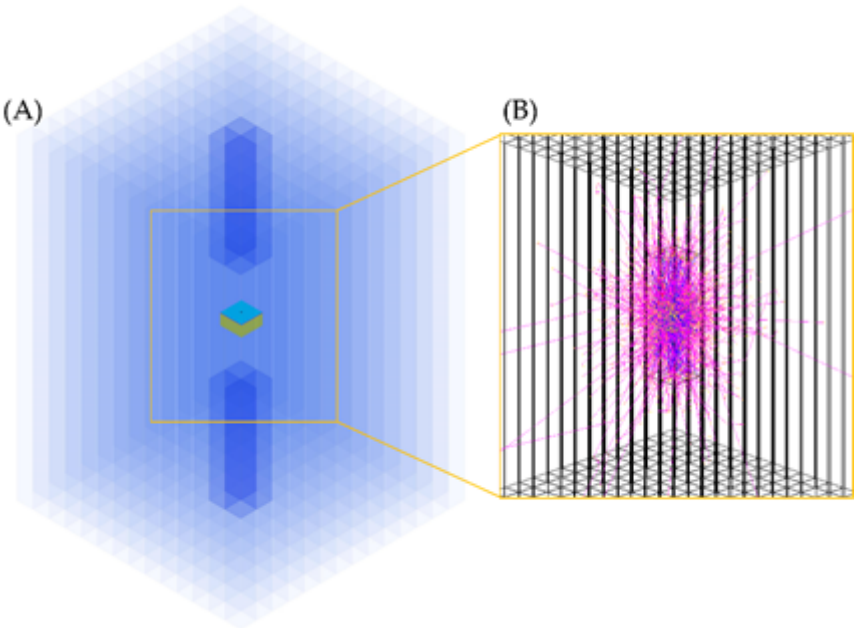

Figure 4

(A) The simulation geometry of the KAPAE detector excluding SiPMs. BGO scintillator bars are shown in blue. The yellow box with a cyan top at the center of the KAPAE detector represents the trigger system including the radioactive source, (B) A simulated 2-γ decay system. Red lines represent tracks of charged particles produced from interactions of γ-rays with the BGO scintillators.

Figure 5

Energy spectra of 511 keV γ-rays from the (A) ^{22}Na source and (B) ^{18}F source simulated using a BGO scintillator in the KAPAE detector. The solid line considers the statistical noise fluctuation, but the dotted line does not. The yellow shade denotes the 2σ range, and the green box denotes the 1σ range. The redline is a Gaussian fit to the data.

Figure 6

The proposed CNN architecture for Ps annihilation localization in the KAPAE detector.